Inorg. Chem. **2006**, *45*, 8736–8742

Reversible Cation/Anion Extraction from $K_2La_2Ti_3O_{10}$: Formation of New Layered Titanates, $KLa_2Ti_3O_{9.5}$ and $La_2Ti_3O_9$

Z. Serpil Gönen,[†] Daniel Paluchowski,[†] Peter Zavalij,[†] Bryan W. Eichhorn,*[,†] and J. Gopalakrishnan[‡]

Department of Chemistry and Biochemistry, Center for Superconductivity Research, University of Maryland, College Park, Maryland 20742, and Solid State and Structural Chemistry Unit, Indian Institute of Science, Bangalore 560012, India

Received March 14, 2006

A new soft-chemical transformation of layered perovskite oxides is described wherein K_2O is sequentially extracted from the Ruddlesden–Popper (R–P) phase, $K_2La_2Ti_3O_{10}$ (**I**), yielding novel anion-deficient $KLa_2Ti_3O_{9.5}$ (**II**) and $La_2Ti_3O_9$ (**III**). The transformation occurs in topochemical reactions of the R–P phase **I** with PPh_4Br and PBu_4Br (Ph = phenyl; Bu = *n*-butyl). The mechanism involves the elimination of KBr accompanied by decomposition of PR_4^+ (R = phenyl or *n*-butyl) that extracts oxygen from the titanate. Analysis of the organic products of decomposition reveals formation of Ph_3PO, Ph_3P, and Ph–Ph for R = phenyl, and Bu_3PO, Bu_3P along with butane, butene, and octane for R = butyl. The inorganic oxides **II** and **III** crystallize in tetragonal structures (**II**: *P*4/*mmm*, $a = 3.8335(1)$ Å, $c = 14.334(1)$ Å; **III**: *I*4/*mmm*, $a = 3.8565(2)$ Å, $c = 24.645(2)$ Å) that are related to the parent R–P phase. **II** is isotypic with the Dion–Jacobson phase, $RbSr_2Nb_3O_{10}$, while **III** is a unique layered oxide consisting of charge-neutral $La_2Ti_3O_9$ anion-deficient perovskite sheets stacked one over the other without interlayer cations. Interestingly, both **II** and **III** convert back to the parent R–P phase in a reaction with KNO_3. While transformations of the R–P phases to other related layered/three-dimensional perovskite oxides in ion-exchange/metathesis/dehydration/reduction reactions are known, the simultaneous and reversible extraction of both cations and anions in the conversions $K_2La_2Ti_3O_{10} \rightleftharpoons KLa_2Ti_3O_{9.5} \rightleftharpoons La_2Ti_3O_9$ is reported here for the first time.

Introduction

Among the several families of nonmolecular inorganic solids, transition metal oxides with perovskite-related structures occupy an important position in view of their wide range of technologically important materials properties. Traditional synthesis of these materials involves high-temperature solid-state reactions of inorganic salts and binary oxides that preclude the chances of obtaining metastable members of the perovskite family. The high temperatures are necessary to overcome the small diffusion rates in solid-state reactions.[1] Current research efforts are therefore directed toward developing alternate low-temperature routes that will enable the synthesis of functionalized metastable perovskite derivatives by way of 'soft' chemical reactions[2] starting from layered perovskite precursors.[3−16]

Two related layered perovskite oxides, the Ruddlesden−Popper (R−P) phases[17] (represented by a general formula $A_2[A'_{n-1}B_nO_{3n+1}]$) and the Dion-Jacobson (D−J) phases[18] (represented by a general formula $A[A'_{n-1}B_nO_{3n+1}]$) are particularly important in this regard due to their ability to undergo ion-exchange, intercalation, and pillaring reactions.

* To whom correspondence should be addressed.
[†] University of Maryland.
[‡] Indian Institute of Science.

(1) Gopalakrishnan, J. *Chem. Mater*. **1995**, *7*, 1265.
(2) Rouxel, J.; Tournoux, M.; Brec, R. Eds. *Soft Chemistry Routes to New Materials-Chimie Douce;* Trans Tech: Aedermannsdorf, Switzerland, 1994.
(3) Schaak, R.; Mallouk, T. *Chem. Mater*. **2002**, *14*, 1455.
(4) Sivakumar, T.; Gopalakrishnan, J. *Mater. Res. Bull*. **2005**, *40*, 39−45.
(5) Viciu, L.; Liziard, N.; Golub, V.; Kodenkandath, T. A.; Wiley, J. B. *Mater. Res. Bull*. **2004**, *39*, 2147−2154.
(6) Neiner, D.; Golub, V.; Wiley, J. B. *Mater. Res. Bull*. **2004**, *39*, 1385−1392.
(7) Sivakumar, T.; Lofland, S. E.; Ramanujachary, K. V.; Ramesha, K.; Subbanna, G. N.; Gopalakrishnan, J. *J. Solid State Chem.* **2004**, *177*, 2635−2638.
(8) Mandal, T. K.; Gopalakrishnan, J. *J. Mater. Chem.* **2004**, *14*, 1273−1280.
(9) Sivakumar, T.; Ramesha, K.; Lofland, S. E.; Ramanujachary, K. V.; Subbanna, G. N.; Gopalakrishnan, J. *Inorg. Chem*. **2004**, *43*, 1857−1864.
(10) Viciu, L.; Golub, V. O.; Wiley, J. B. *J. Solid State Chem.* **2003**, *175*, 88−93.
(11) Panda, M.; Seshadri, R.; Gopalakrishnan, J. *Chem. Mater*. **2003**, *15*, 1554−1559.
(12) Schaak, R. E.; Mallouk, T. E. *J. Am. Chem. Soc*. **2000**, *122*, 2798.
(13) Schaak, R. E.; Mallouk, T. E. *Chem. Mater*. **2000**, *12*, 2513.

10.1021/ic060434g CCC: $33.50
Published on Web 09/21/2006

In these oxides, perovskite sheets of BO_6 octahedra that are n layers thick (n = 1, 2, 3, ...) are interleaved by ion-exchangeable alkali metal (A) cations. Therefore, they are excellent starting materials for the synthesis of metastable derivatives.

Previous studies[19] have shown that ion-exchange/metathesis reactions can be used to transform a R−P phase, $K_2La_2Ti_3O_{10}$, to an Aurivillius phase, $(Bi_2O_2)La_2Ti_3O_{10}$, by reaction with BiOCl at relatively low temperatures (~800 °C). The reverse reaction, the transformation of an Aurivillius phase to the R−P phase, is also possible through a two-step process. The first step requires the removal of the $Bi_2O_2^{2+}$ layer by HCl to form the protonated R−P phase.[20] In the second step, the protonated phase can be converted into the alkali form by a reaction with hot aqueous KOH.[21] BiOCl also reacts with the R−P phase $NaLaTiO_4$ to form a metastable Aurivillius/R−P hybrid material.[22] Similarly, the Wiley group[5,7,23−25] has shown that the oxyhalide lamellar perovskites, $[CuX]LaNb_2O_7$ (X = Cl, Br), and $[FeCl]LaNb_2O_7$ can be obtained by the reaction of a D−J phase, $RbLaNb_2O_7$ with CuX_2 or $FeCl_2$, respectively. Mallouk and co-workers[3,12,13] showed that these materials could be exfoliated in novel acid−base reactions. For example, the protonated analogues of these phases, such as $HLaNb_2O_7$ and $H_2Ca_2Ta_2TiO_{10}$, form single-layer sheets or scrolls when reacted with NBu_4OH (Bu = butyl). Furthermore, it is possible to perform condensation/dehydration reactions with protonated forms of both the series, yielding three-dimensional A-site defective perovskites.[15]

Soft chemical ion-exchange reactions are also a useful means to convert R−P phases to D−J phases. For example, the D−J $M^{II}La_2Ti_3O_{10}$ phases (M = Co, Cu, Zn) were prepared[26] by the reaction of the $Na_2La_2Ti_3O_{10}$ R−P precursor with MCl_2. The corresponding M = Pb, Ba, Sr, and VO derivatives were prepared[19] similarly by the reaction of $K_2La_2Ti_3O_{10}$ with $MCl_2/VOSO_4{\cdot}3H_2O$. Conversion of a D−J-type phase to a R−P-type phase has also been carried out. Armstrong and Anderson[27] prepared $Rb_2LaNb_2O_7$ by reaction of $RbLaNb_2O_7$ with Rb vapor. $Li_2LaTa_2O_7$, $Li_2Ca_2Ta_3O_{10}$, and $Na_2Ca_2Ta_3O_{10}$ were prepared similarly from the corresponding D−J phases by reductive insertion of alkali metals using n-BuLi or NaN_3.[28]

Most of the soft-chemical transformations involving layered perovskite oxides described above are *irreversible* cation exchange processes.[3] Herein we describe a new type of topochemical process involving the reaction between the R−P oxide $K_2La_2Ti_3O_{10}$ and PR_4Br salts (R = Ph, n-Bu) wherein interlayer potassium ions and oxide ions from the perovskite slabs are extracted in a concerted manner to yield the metastable products $KLa_2Ti_3O_{9.5}$ (D−J) and $La_2Ti_3O_9$ (layered perovskite). More importantly, the process is entirely *reversible* in the sense that both the layered perovskites $KLa_2Ti_3O_{9.5}$ and $La_2Ti_3O_9$ could be transformed back into the parent $K_2La_2Ti_3O_{10}$. We have also established the crystal structures of both the intermediate phases. The reactivity of the $La_2Ti_3O_9$ phase is significantly higher than $La_2Ti_3O_9$ prepared from dehydration of $H_2La_2Ti_3O_{10}$.[29]

Experimental Section

Synthesis. General. La_2O_3 was dried at 950 °C for 24 h before each use. The other oxides and carbonate precursors (Cerac Inorganics) were used without further purification. Tetraphenylphosphonium bromide, PPh_4Br (97%), and tetrabutylphoshonium bromide PBu_4Br, were purchased from Aldrich. Both compounds were dried at 200 °C under high vacuum for 6 h and stored in a nitrogen-filled drybox.

$K_2La_2Ti_3O_{10}$. The compound was prepared from stoichiometric mixtures of La_2O_3 and TiO_2 with excess KNO_3 according to the published procedure.[19] Excess (25 mol %) KNO_3 was added to compensate the loss due to volatilization. The mixture was heated at 1000 °C for 6 h with a temperature ramp of 1 °C/min twice with one intermediate grinding. After the reaction, the product was washed with distilled water and dried at 500 °C to obtain the anhydrous white polycrystalline product.

$KLa_2Ti_3O_{9.5}$. A 1:1 (molar ratio) mixture of $K_2La_2Ti_3O_{10}$ (0.200 g) and PPh_4Br (0.131 g) was intimately ground in a Wig-L-Bug bug and placed into a Pyrex tube inside the drybox. The tube was then sealed under high vacuum, and the mixture was heated at 300 °C for 72 h. The product was washed with distilled water and acetone several times to remove the KBr and the organic byproducts. After being washed, the white, polycrystalline product was dried in air at 120 °C for ca. 1 h. The same procedure was used to prepare the title compound from PBu_4Br and $K_2La_2Ti_3O_{10}$. ***CAUTION**: The reaction generates volatile organic gases and reaction tubes are pressurized after reaction. Tubes should be handled behind a blast shield and cooled in liquid nitrogen before opening.*

$La_2Ti_3O_9$. In a similar reaction, a 1:2.5 molar mixture of $K_2La_2Ti_3O_{10}$ (0.200 g) and PPh_4Br (0.328 g) was intimately ground using a Wig-L-Bug bug and placed into a Pyrex tube inside the nitrogen box. The 20% excess PPh_4Br was added to ensure complete reaction. The tube was sealed under vacuum, and the mixture was heated at 300 °C for 72 h. The product was washed with copious amounts of distilled water and acetone to remove the byproducts. After being washed, the white, polycrystalline product was dried in air at 120 °C for ca. 1 h. The same procedure was used to prepare the title compound from PBu_4Br and $K_2La_2Ti_3O_{10}$. ***CAUTION**: The reaction generates volatile organic gases and reaction tubes are*

(14) Schaak, R. E.; Mallouk, T. E. *Chem. Mater.* **2000**, *12*, 3427.
(15) Schaak, R. E.; Mallouk, T. E. *J. Solid State Chem.* **2000**, *155*, 46.
(16) Schaak, R. E.; Guidry, E. N.; Mallouk, T. E. *Chem. Commun.* **2001**, 853.
(17) Ruddlesden, S. N.; Popper, P. *Acta Crystallogr.* **1957**, *10*, 538. Ruddlesden, S. N.; Popper, P. *Acta Crystallogr.* **1958**, *11*, 54.
(18) (a) Dion, M.; Ganne, M.; Tournoux, M. *Mater. Res. Bull.* **1981**, *16*, 1429. (b) Jacobson, A. J.; Johnson, J. W.; Lewandowski, J. T. *Inorg. Chem.* **1985**, *24*, 3727
(19) Gopalakrishnan, J.; Sivakumar, T.; Ramesha, K.; Thangadurai, V.; Subbanna, G. N. *J. Am. Chem. Soc.* **2000**, *122*, 6237.
(20) Sugimoto, W.; Shirata, M.; Sugahara, Y.; Kuroda, K. *J. Am. Chem. Soc.* **1999**, *121*, 11601.
(21) Schaak, R. E.; Mallouk, T. E. *J. Solid State Chem.* **2001**, *161*, 225.
(22) Sivakumar, T.; Seshadri, R.; Gopalakrishnan, J. *J. Am. Chem. Soc.* **2001**, *123*, *11496.*
(23) Kodenkandath, T. A.; Lalena, J. N.; Zhou, W. L.; Carpenter, E. E.; Sangregorio, C.; Falster, A. U.; Simmons, W. B., Jr.; O'Connor, C. J.; Wiley, J. B. *J. Am. Chem. Soc.* **1999**, *121*, 10743.
(24) Kodenkandath, T. A.; Kumbhar, A. S.; Zhou, W. L.; Wiley, J. B. *Inorg. Chem.* **2001**, *40*, 710.
(25) Viciu, L.; Koenig, J.; Zhou, L.; Wiley, J. B. *Chem. Mater.* **2003**, *15*, 1480.
(26) Hyeon, K.; Byeon, S. *Chem. Mater.* **1999**, *11*, 352.
(27) Armstrong, A. R.; Anderson, P. A. *Inorg. Chem.* **1994**, *33*, 4366.
(28) Toda, K.; Takahashi, M.; Teranishi, T.; Ye, Z. G.; Sato, M.; Hinatsu, Y. *J. Mater. Chem.* **1999**, *9*, 799.
(29) Gopalakrishnan, J.; Bhat, V. *Inorg. Chem.* **1987**, *26*, 4301.

pressurized after reaction. Tubes should be handled behind a blast shield and cooled in liquid nitrogen before opening.

Analysis of Volatiles. The byproducts of the previous reactions were evaluated by freezing the sealed reaction tubes in liquid nitrogen, opening the tubes, and extracting the soluble components with CH_2Cl_2 or acetone at low temperature. After the filtration of the particulates, the solutions containing the soluble byproducts were analyzed by NMR and MS studies (see below).

Dehydration Reaction. $H_2La_2Ti_3O_{10}$ was prepared according to published procedures.[29] $K_2La_2Ti_3O_{10}$ was stirred in a 0.1 M HNO_3 solution at 60 °C for 48 h. The aqueous solution was then decanted, leaving an extremely crystalline white powder. X-ray powder diffraction (XRD) was used to verify the product identity as that of $H_2La_2Ti_3O_{10}$. Subsequently, this oxide was dehydrated at 250 °C under dynamic vacuum for 48 h to yield a white crystalline powder, $La_2Ti_3O_9$ (XRD).

Reactions with KNO_3. $KLa_2Ti_3O_{9.5}$ and $La_2Ti_3O_9$ prepared through cation/anion extraction reactions were treated with excess (10:1) KNO_3 at 600 °C for 72 h with a temperature ramp of 1 °C/min. XRD analysis of the reactions showed complete conversion to $K_2La_2Ti_3O_{10}$.

Thermal Reactions. $KLa_2Ti_3O_{9.5}$ and $La_2Ti_3O_9$ were heated at 1000 °C in air for 24 h. $La_2Ti_3O_9$ converts to the A-site defective perovskite, $La_{2/3}TiO_3$,[29,30] and $KLa_2Ti_3O_{9.5}$ disproportionates to give a mixture of $La_{2/3}TiO_3$ and $K_2La_2Ti_3O_{10}$.

Characterization. XRD patterns were recorded using either a Bruker D8 Advance X-ray powder diffractometer (Cu Kα radiation, $\theta-\theta$, KEVEX detector) or a C2 Discover equipped with a HiStar Detector. Powder patterns were obtained with 12 h runs using a step width of 0.02° between $3° \leq 2\theta \leq 90°$. The cell parameters were indexed using JADE 5.1. The Rietveld refinement (GSAS/EXPGUI software)[31,32] was conducted using modified pseudo-Voigt (Thompson−Cox−Hastings) profile shape functions. Initial atomic coordinates for $Nd_2Ti_3O_9$[33] were used as a model for $La_2Ti_3O_9$. A summary of the crystal data and the Rietveld refinement data can be found in the Supporting Information.

Energy-dispersive X-ray spectroscopy (EDS) (150 eV resolution) and wavelength dispersive spectroscopy (WDS) (15 keV accelerating voltage, 2×10^{-8} A current, ZAF corrections) analyses were performed by using a JEOL JXA-8900 microprobe analyzer. For the WDS analysis, $K_2La_2Ti_3O_{10}$ was used as a standard. Selected area electron diffraction (SAED) patterns were acquired using a Philips CM300FEG transmission electron microscope (TEM) operated at 297 kV and Kodak SO-163 electron film. After being sonicated in ethanol for 5 min, particle suspensions were drop-mounted onto Cu TEM grids with Quantifoil amorphous carbon support films while sitting on filter paper. Electron diffraction patterns were acquired at a camera length of 1.75 m. TEM images were obtained with a ZEISS EM 10CA TEM operated at 80 kV. SAED simulations were performed using the EMS online Electron Microscopy Image Simulation program at http://cimewww.epfl.ch. High-resolution scanning electron microscopy (SEM) experiments were performed on a field-emission Hitachi S4700-FE scanning electron microscope.

^{31}P NMR spectra were recorded from acetone solutions on a Bruker DRX400 spectrometer operating at 162 MHz. The ^{31}P NMR data were referenced against an external 85% H_3PO_4/CD_2Cl_2 standard (0 ppm). IR spectra were recorded from KBr pellets on a Nicolet 560 FTIR spectrometer using a KBr-to-product ratio of 100:4 (w/w). Gas chromatographic analysis was performed on an HP 5890 gas chromatograph equipped with a flame ionization detector using a 25 m methyl silicone column. GC-MS experiments were conducted on a Shimadzu QP5000MS coupled with a GC17A gas chromatograph.

Results

Synthesis and Characterization. We have investigated the reactions between $K_2La_2Ti_3O_{10}$ and PPh_4Br in the solid state in 1:1 and 1:2 molar ratios. $K_2La_2Ti_3O_{10}$ reacts with 1 and 2 molar equiv of PPh_4Br to form $KLa_2Ti_3O_{9.5}$ and $La_2Ti_3O_9$, with the formal extraction of 1/2 and 1 mol of K_2O, respectively. During the reactions, PPh_4^+ reacts with the titanate to give Ph_3PO, PPh_3, and Ph_2, whereas Br^- reacts with the lattice K^+ ions to form KBr. A stacked plot of the XRD profiles of the various compounds is given in the Supporting Information (Figure S-1). The balanced equations (1 and 2) for the reactions are

$$K_2La_2Ti_3O_{10} + PPh_4Br \rightarrow KLa_2Ti_3O_{9.5} + KBr + 1/2PPh_3O + 1/2PPh_3 + 1/2Ph_2 \quad (1)$$

$$K_2La_2Ti_3O_{10} + 2PPh_4Br \rightarrow La_2Ti_3O_9 + 2KBr + PPh_3O + PPh_3 + Ph_2 \quad (2)$$

The products and byproducts were characterized by several analytical methods. The oxides, $KLa_2Ti_3O_{9.5}$ and $La_2Ti_3O_9$, were characterized by EDS, WDS, SAED, SEM, and Rietveld refinement of powder XRD data (see structural analysis section). The KBr formed in reactions 1 and 2 was clearly evident in the powder XRD patterns of the unwashed reaction product mixtures. The biphenyl from eq 1 was extracted into acetone and characterized by GC and GC-MS through comparisons with authentic samples. The 1:1 molar ratios of PPh_3 and Ph_3PO formed in the reactions were determined by quantitative integration of the ^{31}P NMR resonances recorded from acetone extracts of the reaction products. IR spectral analysis of the unwashed reaction products showed the characteristic P═O stretch of PPh_3O at 1190 cm^{-1}.

EDS analysis of washed $KLa_2Ti_3O_{9.5}$ confirmed the presence of K, La, and Ti. Similar analysis of washed $La_2Ti_3O_9$ showed only the presence of La and Ti. Phosphorus was detected in both samples at low concentrations; however, bromine was not. Because of the overlap of La and Ti lines in the EDS spectrum, WDS analysis was carried out on the final washed products to determine the quantitative elemental composition. $K_2La_2Ti_3O_{10}$ was used as a standard reference in the WDS analysis. The formulas were determined from the elemental ratios of the heavy atoms together with the required idealized oxygen contents for the fully oxidized metal ions. The resulting compositions $K_{1.10(5)}La_{2.05(3)}Ti_{2.97(3)}O_{9.5}$ and $La_{2.05(2)}Ti_{2.96(2)}O_9$ are in excellent agreement with the ideal formulas $KLa_2Ti_3O_{9.5}$ and $La_2Ti_3O_9$.

SEM images (Figure 1) show that the $K_2La_2Ti_3O_{10}$ precursor and $La_2Ti_3O_9$ product have almost identical morphol-

(30) MacEachern, M. J.; Dabkowska, H.; Garrett, J. D.; Amow, G.; Gong, W.; Liu, G.; Greedan, J. E. *Chem. Mater.* **1994**, *6*, 2092.
(31) Larson A. C.; Von Dreele R. B. *General Structure Analysis System (GSAS)*; Los Alamos National Laboratory Report LAUR 86-748, 2000. Toby B. H. *J. Appl. Cryst.* **2001**, *34*, 210−213.
(32) Coelho, A. A. *J. Appl. Crystallogr.* **2000**, *33*, 899.
(33) Richard, M.; Brohan, L.; Tournoux, M. *J. Solid State Chem.* **1994**, *112*, 345.

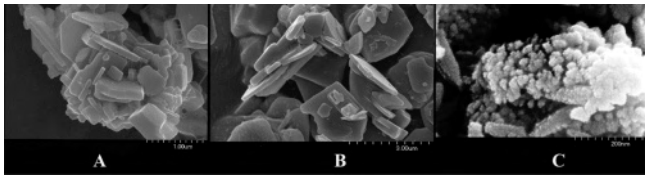

Figure 1. High-resolution SEM micrographs. (A) $K_2La_2Ti_3O_{10}$, (B) $La_2Ti_3O_9$ via the topochemical process, and (C) $La_2Ti_3O_9$ via dehydration of $H_2La_2Ti_3O_{10}$.

ogies and size. The platelike crystallites are 0.1−0.3 μm thick and <5 μm across. The large aspect ratios are consistent with their layered structure and XRD profiles (see next sections). SEM studies indicate that the extraction of K_2O from $K_2La_2Ti_3O_{10}$ to give the $La_2Ti_3O_9$ product occurs topochemically with no apparent change in particle size or morphology.

To examine the possible sources of the phosphorus impurity, reactions between $K_2La_2Ti_3O_{10}$ and PBu_4Br were investigated. Similarly, $K_2La_2Ti_3O_{10}$ reacts with 1 and 2 molar equiv of PBu_4Br to form $KLa_2Ti_3O_{9.5}$ and $La_2Ti_3O_9$, with the formal extraction of 1/2 and 1 mol of K_2O, respectively. Because the radical decomposition mechanism of the PBu_4^+ differs from that of PPh_4^+, the byproducts of the PBu_4^+ reaction were different. The reactions are shown in eqs 3 and 4 below.

$$K_2La_2Ti_3O_{10} + PBu_4Br \rightarrow KLa_2Ti_3O_{9.5} + KBr + 1/2Bu_3PO + 1/2PBu_3 + (1/2 - x)C_4H_{10} + (1/2 - x)C_4H_8 + xC_8H_{18}\ (0 < x < 1/2) \quad (3)$$

$$K_2La_2Ti_3O_{10} + 2PBu_4Br \rightarrow La_2Ti_3O_9 + 2KBr + Bu_3PO + PBu_3 + (1 - x)C_4H_{10} + (1 - x)C_4H_8 + xC_8H_{18}\ (0 < x < 1) \quad (4)$$

GC and GC-MS studies revealed that the butyl radical decomposition gives equal quantities of butane and butene resulting from hydrogen atom extraction. In addition, trace amounts of the radical coupling product, octane, were also detected.

EDS analysis of washed $KLa_2Ti_3O_{9.5}$ confirmed the presence of K, La, and Ti. Similar analysis of washed $La_2Ti_3O_9$ showed only the presence of La and Ti. Phosphorus and bromide were not detected in these samples. XRD analysis produced diffraction patterns identical to those of the above reactions with PPh_4Br.

Thermal Stability Studies. Both of the new compounds are thermally unstable at high temperatures. $La_2Ti_3O_9$ irreversibly converts to the known[29,30] three-dimensional defect perovskite $La_{2/3}TiO_3$ after heating at 1000 °C for 24 h. It should be noted that this synthesis temperature is significantly lower than the 1400 °C reaction temperature required for the direct synthesis of $La_{2/3}TiO_3$ from La_2O_3 and TiO_2.[30] In addition, $La_{2/3}TiO_3$ is unreactive toward KNO_3 (see next section). On heating at 1000 °C, $KLa_2Ti_3O_{9.5}$ disproportionates according to eq 5.

$$2KLa_2Ti_3O_{9.5} \rightarrow K_2La_2Ti_3O_{10} + 3La_{2/3}TiO_3 \quad (5)$$

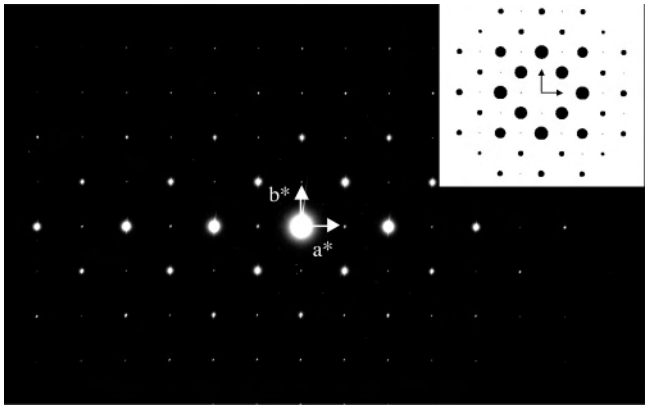

Figure 2. Observed and simulated (inset) ED patterns of $KLa_2Ti_3O_{9.5}$.

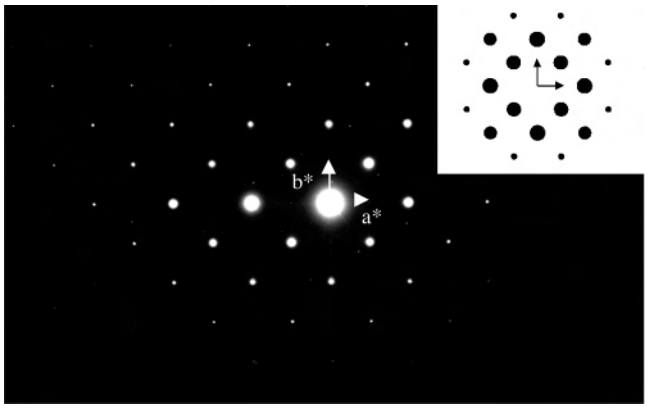

Figure 3. Observed and simulated (inset) ED patterns of $La_2Ti_3O_9$.

Reactivity Studies. Both $KLa_2Ti_3O_{9.5}$ and $La_2Ti_3O_9$ react with excess KNO_3 in the solid state at $T \leq 600$ °C in air to reform the parent $K_2La_2Ti_3O_{10}$ (see Figure S-1). We compared the reactivity of $La_2Ti_3O_9$ described here with that prepared by the known dehydration method previously described[29] (see Experimental Section). The $La_2Ti_3O_9$ obtained from dehydration has significantly smaller particle size (∼10−20 nm, Figure 1c) and gives broad diffraction peaks relative to that prepared from eqs 2 and 4. The XRD peak intensities and peak positions are otherwise the same. Surprisingly, the dehydration $La_2Ti_3O_9$ shows no reactivity toward KNO_3 regardless of the reaction time at temperatures as high as 650 °C, which is in sharp contrast to the reactivity of $La_2Ti_3O_9$ prepared by our method.

Structural Analysis. SAED was used to determine the symmetry and estimate the unit cell parameters of both $KLa_2Ti_3O_{9.5}$ and $La_2Ti_3O_9$. The [001] zone axes of SAED data together with simulated patterns are shown in Figures 2 and 3, respectively. The indexed patterns are given in the supporting material. The SAED data indicate that both of the compounds have tetragonal symmetry. For $KLa_2Ti_3O_{9.5}$, the [001] zone axis indicates a primitive cell with no systematic absences. In contrast, the [001] zone axis pattern of $La_2Ti_3O_9$ reveals the reflection conditions $hk0$, $h + k = 2n$ and $0k0$, $k = 2n$, which is consistent with a body-centered unit cell. Although several crystallites were studied, we only observed [001] zone axes due to the preferred orientation of the crystallites in the Cu grids.

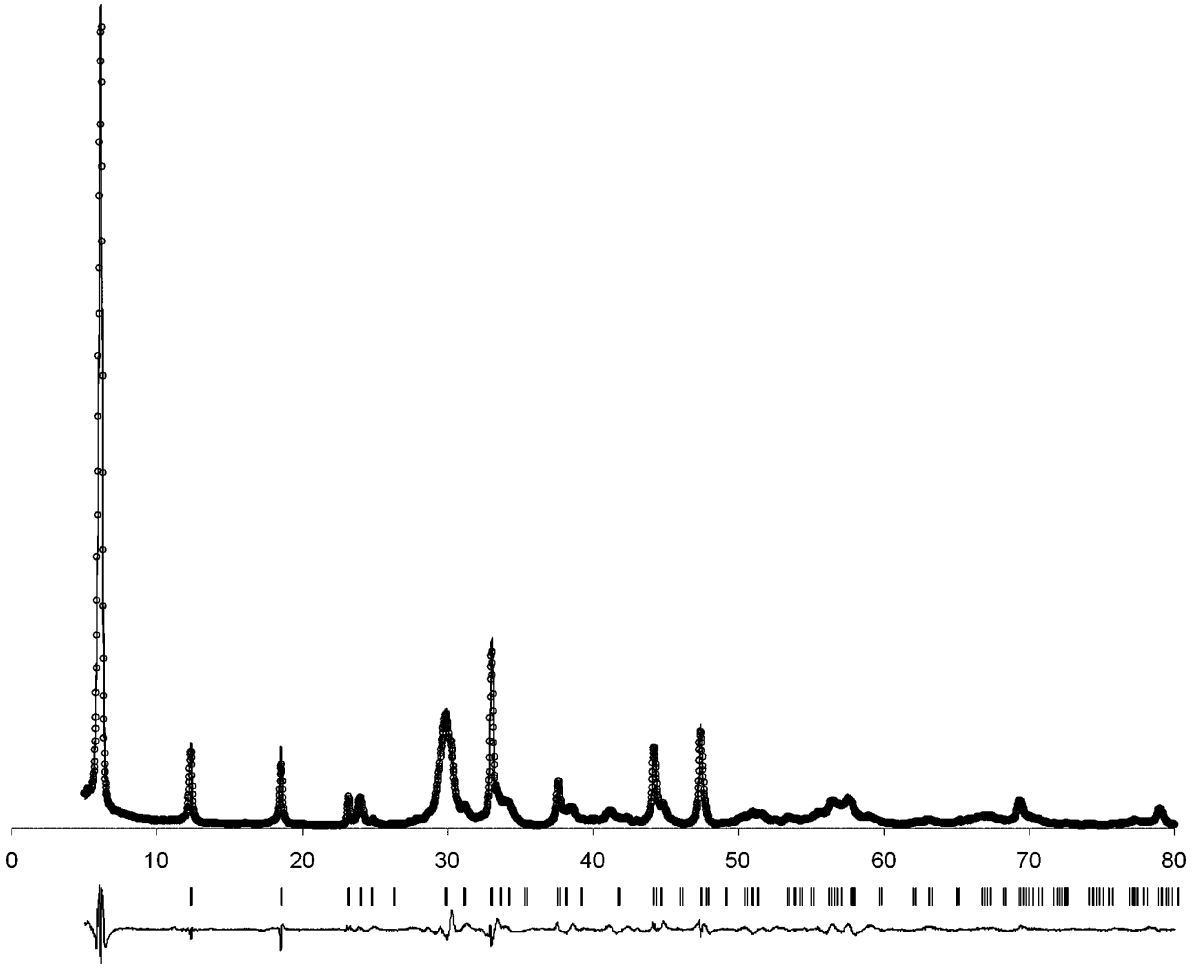

Figure 4. Observed (circles), calculated (line), and difference (bottom) XRD profiles of $KLa_2Ti_3O_{9.5}$. The tick marks show the allowed reflections for $KLa_2Ti_3O_{9.5}$ (bottom).

The XRD patterns of both products indicate layered structures with strong, low-angle 00*l* reflections (the 001 reflection for $KLa_2Ti_3O_{9.5}$; the 002 for $La_2Ti_3O_9$), which are consistent with the SEM the SAED results showing strong preferred orientations. The XRD profiles (and Rietveld refinements) for each compound are shown in Figures 4 and 5, respectively. The indexed tetragonal unit cells (see Table 1) show contraction along the *c* direction as K_2O is systematically removed from the structure. Note that the cell of $H_2La_2Ti_3O_{10}$ is intermediate to those of $La_2Ti_3O_9$ and $KLa_2Ti_3O_{9.5}$, as expected from size and charge considerations.

Structural analyses of $KLa_2Ti_3O_{9.5}$ and $La_2Ti_3O_9$ were performed by comparing the XRD patterns of these compounds to those of the known phases. Rietveld profile analyses of the XRD data were complicated by the broadness of the peaks and the presence of O vacancies, which could not be determined by XRD. The D−J perovskite oxide $RbSr_2Nb_3O_{10}$[34] was used as a structural model for $KLa_2Ti_3O_{9.5}$ due to the similarities of the respective XRD patterns and refined unit cells. $RbSr_2Nb_3O_{10}$ is a member of D−J family of compounds with a single layer of Rb^+ cations between the $[Sr_2Nb_3O_{10}]^{-1}$ triple perovskite layers. The crystal lattice is tetragonal, space group *P4/mmm*, with unit cell parameters of $a = 3.8944(2)$ Å and $c = 15.2710(8)$ Å. Except for the 5% oxygen vacancy, $KLa_2Ti_3O_{9.5}$ is isostructural to $RbSr_2Nb_3O_{10}$ with very similar cell parameters ($a = 3.8335(1)$ Å, $c = 14.334(1)$ Å) and atomic positions.[34] A polyhedral representation of the $KLa_2Ti_3O_{9.5}$ structure is shown in Figure 6b. The refined atomic coordinates are given in Table 2. In $KLa_2Ti_3O_{9.5}$, the $[La_2Ti_3O_{9.5}]^{-1}$ triple perovskite slabs are positioned directly on top of each other with K^+ ions in the eight-coordinate sites between the layers. The alignment of the $[La_2Ti_3O_{9.5}]^{-1}$ layers represents a shift of 1/2, 1/2, 0 relative to the parent $K_2La_2Ti_3O_{10}$ (see Figure 6a).

The structure of $La_2Ti_3O_9$ was initially modeled after that of $Nd_2Ti_3O_9$, which was obtained from the dehydration of $H_2Nd_2Ti_3O_{10}$.[33] The Rietveld refinement of the heavy atom positions using $Nd_2Ti_3O_9$ model gave poor fits to the experimental data and was inconsistent with SAED results and the reactivity of the compound. A new model was constructed in which the $[La_2Ti_3O_{9.5}]^{-1}$ slabs were shifted back by 1/2, 1/2, 0 and an additional 5% oxygen vacancy was introduced to give $La_2Ti_3O_9$. This model gives superior fits (Figure 5) and is consistent with expectations based on the K_2O elimination in the formation of $KLa_2Ti_3O_{9.5}$ and the fact that $La_2Ti_3O_9$ readily reacts with KNO_3 to re-form the $K_2La_2Ti_3O_{10}$ starting material. The refined atomic coordinates are given in Table 2. A ball-and-stick drawing of the model

(34) Thangadurai, V.; Schmid-Beurmann, P.; Weppner, W. *J. Solid State Chem.* **2001**, *158*, 279.

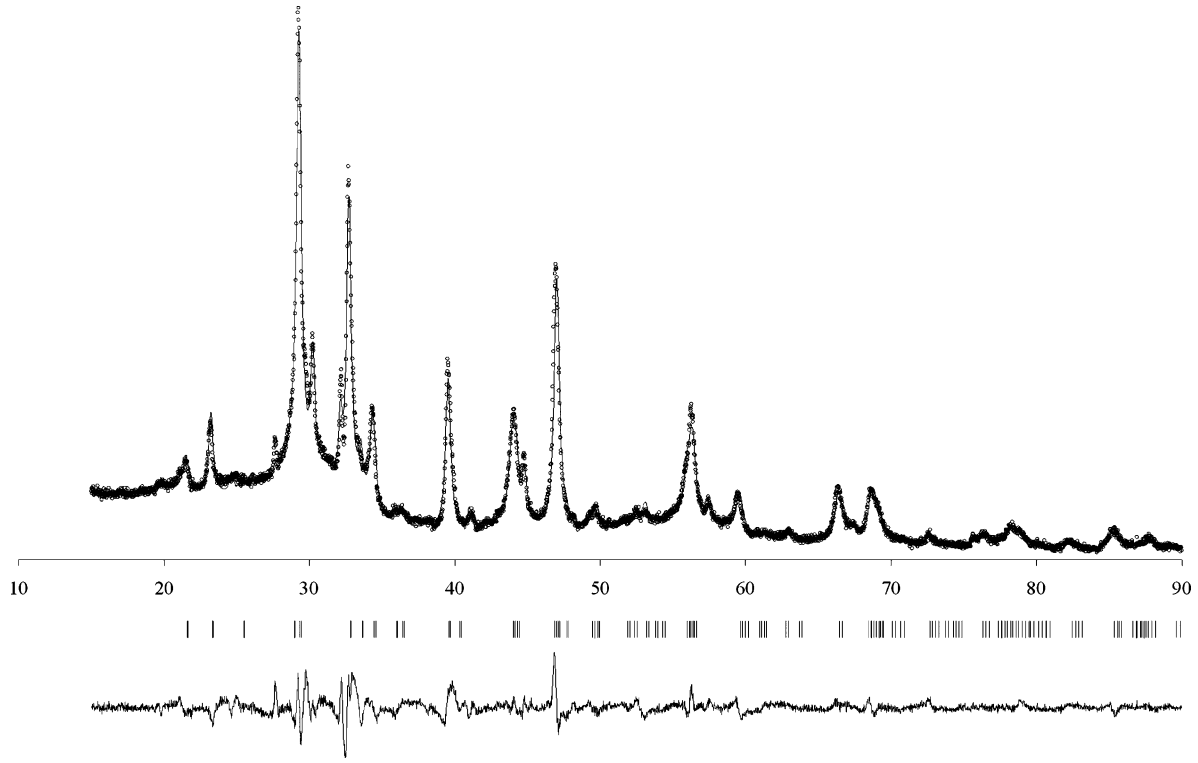

Figure 5. Observed (circles), calculated (line) and difference (bottom) XRD profiles of $La_2Ti_3O_9$. The tick marks show the allowed reflections for $La_2Ti_3O_9$ (bottom).

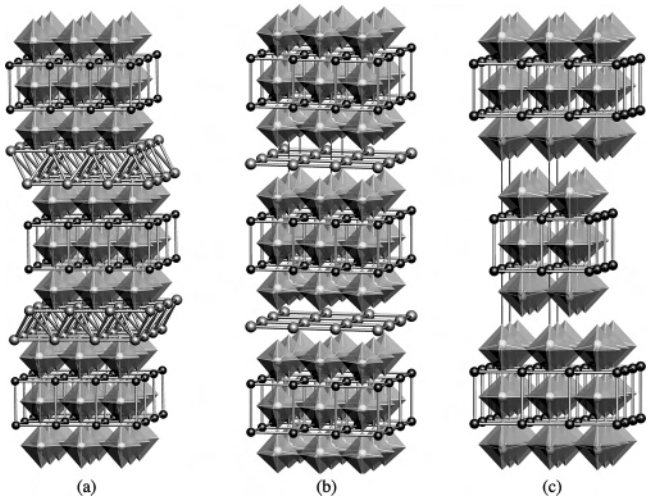

Figure 6. Polyhedral drawings of (a) $K_2La_2Ti_3O_{10}$, (b) $KLa_2Ti_3O_{9.5}$, and (c) $La_2Ti_3O_9$. K^+ ions are large gray spheres, La^{3+} ions are small black spheres, TiO_6 octahedra are gray.

Table 1. Crystallographic Data for $KLa_2Ti_3O_{9.5}$, $La_2Ti_3O_9$, and Related Compounds

	$K_2La_2Ti_3O_{10}$[a]	$KLa_2Ti_3O_{9.5}$	$La_2Ti_3O_9$	$H_2La_2Ti_3O_{10}$[b]
space group	*I*4/*mmm*	*P*4/*mmm*	*I*4/*mmm*	*I*4/*mmm*
a[c](Å)	3.8769(1)	3.8335(1)	3.8565(2)	3.824
c[c](Å)	29.824(1)	14.334(1)	24.645(2)	27.4
R_{wp} (%)	10.19	11.51	6.86	–
R_p (%)	2.73	8.9	5.2	–
Bragg-R (%)	1.46	5.79	13.24	–

[a] References 29 and 38. [b] Reference 29.

structure is given in Figure 6c. The reported structure of $Nd_2Ti_3O_9$ contains Nd^{3+} ions disordered on the O4 sites (see Figure 7) which gives rise to short Nd−Ti separations.[33] In contrast, our refinement results indicated that all of the La^{3+} cations remained in the perovskite layers and there was no migration to the interlayer areas. Moreover, this structure is a logical progression in the $K_2La_2Ti_3O_{10} \rightarrow KLa_2Ti_3O_{9.5} \rightarrow La_2Ti_3O_9$ series.

Table 2. Fractional Coordinates for $KLa_2Ti_3O_{9.79}$ and $La_2Ti_3O_9$

atom	x	y	z	occ.
		$KLa_2Ti_3O_{9.5}$		
K1	0.5	0.5	0.5	1
La1	0.5	0.5	0.1481 (1)	1
Ti1	0	0	0	1
Ti2	0	0	0.2752(6)	1
O1	0	0.5	0	1
O2	0	0	0.1402(6)	0.893(16)
O3	0	0.5	0.2914(7)	1
O4	0	0	0.4112(6)	1
		$La_2Ti_3O_9$		
La1	0	0	0.4157(3)	1
Ti1	0	0	0	1
Ti2	0	0	0.1710(6)	1
O1	0	0.5	0	0.5
O2	0	0	0.074(2)	1
O3	0	0.5	0.154(1)	1
O4	0	0	0.237(2)	1

As mentioned previously, the stoichiometries of the compounds require vacancies in the oxygen positions. There are four different oxygen positions in the perovskite layers of both compounds as shown in Figure 6b and c. Unfortunately, Rietveld analyses of XRD data do not give reliable results for oxygen positions and/or vacancies, and we are uncertain about the nature of the defects at this time. Therefore, neutron diffraction is necessary to determine O vacancy positions satisfactorily.

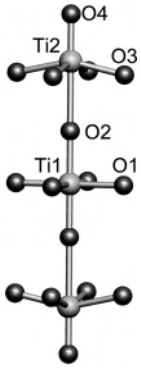

Figure 7. Ball-and-stick representation of corner-shared TiO_6 octahedra in the perovskite layers of $La_2Ti_3O_9$.

Discussion

Reactions 1−4 involve formal extraction of K_2O from the parent $K_2La_2Ti_3O_{10}$. The ability to extract K_2O relies on the unique ability of PR_4^+ cations (R = Ph, Bu) to react with and remove lattice oxide. The reaction is best understood by examining the two half-reactions describing the extraction of lattice K^+ and O^{2-} in the PPh_4^+ system:

$$K^+ + Br^- \rightarrow KBr \quad (6a)$$

$$2PPh_4^+ + O^{2-} \rightarrow Ph_3PO + Ph-Ph + PPh_3 \quad (6b)$$

In addition to the formation of KBr, which is the driving force as in many low-temperature ionic metathesis reactions, the present chemistry has the added enthalpic advantage of P═O bond formation. The thermodynamics of the PBu_4^+ system are quite similar. However, in addition to alkyl coupling to give octane, the alkyl radical elimination pathway allows for the formation of alkane and alkene, a process not available to PPh_4^+.

The phosphorus impurities associated with the PPh_4^+ reactions presumably resulted from the insolubility of Ph_3PO, which could not fully be washed out of the sample. While the PBu_4^+ reactions gave more soluble byproducts and alleviated the P contamination product, the butyl system was also more prone to additional degradation and frequently generated small quantities of elemental red phosphorus that sublimed to the cold end of the reaction ampule.

While topochemical cation exchange is relatively common, anion removal and/or exchange is less common.[35] Anion exchange can be virtually thermoneutral, although large kinetic barriers may exist. Oxide ion conductors[36] are examples of fast anion-exchange materials, although high temperatures are usually required. Anion extractions, however, require a simultaneous reduction of the host lattice and demand a high price in lattice energy. Apparently, the energetics of reactions 6a and 6b adequately compensate for these requirements, facilitating reactions 1−4. In a subsequent publication, we will show that similar reactions involving D−J niobates proceed by KBr formation coupled with Br^-/O^{2-} exchange. These reactions are quite different from the cation metathesis and acid−base chemistry known for the layered early transition metal perovskites and provide access to new types of low-temperature phases.

In summary, we have described the synthesis of two new perovskites, $KLa_2Ti_3O_{9.5}$ and $La_2Ti_3O_9$, through the use of a new type of topochemical anion extraction method. More importantly, their formation demonstrates that *reversible* interconversions of various classes of perovskites can occur in low-temperature transformations. The reactions:

$$R-P \rightleftharpoons D-J \rightleftharpoons \text{layered perovskite} \rightarrow \text{perovskite}$$

have been documented in the forward direction in irreversible transformations, but the interconversion of all members in this class within a single series of compounds is new.

The structures of the new compounds, $KLa_2Ti_3O_{9.5}$ and $La_2Ti_3O_9$, are anion-deficient variants of known perovskite phases. $KLa_2Ti_3O_{9.5}$ adopts the $RbSr_2Nb_3O_{10}$ structure with eight-coordinate K^+ between the layers. $La_2Ti_3O_9$ is a variant of the $Nd_2Ti_3O_9$ structure but with a different cation ordering motif. The layered framework with the empty interlayer gallery suggests that $La_2Ti_3O_9$ could be a starting material for a number of intercalation/exfoliation reactions, while the existence of oxygen vacancies could give rise to a high oxide-ion conduction in this material.

Acknowledgment. We are grateful to the NSF-DMR for support of this work and the LINK Foundation Fellowship for Z.S.G. We gratefully thank Banu Kesanli and Suzanne Bogaczyk for the help with NMR and GC analyses, respectively. We are indebted to Dr. John Henry Scott[37] and Tim Maugel for the expert electron microscopy studies. The work at Bangalore is supported by DST, Government of India.

Supporting Information Available: A summary of Rietveld refinement data, a stacked plot of the XRD data showing the interconversions of the various phases and indexed electron diffraction data. This material is available free of charge via the Internet at http://pubs.acs.org.

IC060434G

(35) Stoltz, C.; Ramesha, K.; Sirchio, S. A.; Gönen, Z. S.; Eichhorn, B. W.; Salamanca-Riba, L.; Gopalakrishnan, J. *J. Am. Chem. Soc.* **2003**, *125*, 4285.
(36) Islam, M.; Davies, R. *J. Mater. Chem.* **2004**, *14*, 86.
(37) Certain commercial equipment, instruments, or materials are identified in this paper in order to specify the experimental procedure adequately. Such identification is not intended to imply recommendation or endorsement by the National Institute of Standards and Technology, nor is it intended to imply that the materials or the equipment identified are necessarily the best available for the purpose.
(38) Toda, K.; Watanabe, J.; Sato, M. *Mater. Res. Bull.* **1996**, *31*, 1427.